

Article

Effects of Fine Particles on Thermal Conductivity of Mixed Silica Sands

Jaehun Ahn ¹ and Jongwon Jung ^{2,*}

¹ Department of Civil and Environmental Engineering, Pusan National University, 2 Busandaehak-ro 63beon-gil, Geumjeong-gu, Busan 46241, Korea; jahn@pusan.ac.kr

² School of Civil Engineering, Chungbuk National University, 1 Chungdae-ro, Seowon-Gu, Cheongju, Chungbuk 28644, Korea

* Correspondence: jjung@chungbuk.ac.kr; Tel.: +82-43-261-2405

Academic Editor: Peter Van Puyvelde

Received: 17 April 2017; Accepted: 17 June 2017; Published: 23 June 2017

Abstract: The physical properties of granular materials (such as hydraulic, strength, and thermal properties) are largely dependent on their density (or porosity) and particle size distribution. In infrastructure design, the thermal properties of soils are now more important than in the past. However, our understanding of the thermal properties of mixed granular materials is still poor. In this study, the thermal conductivity of silica sands with different porosities and particle sizes was experimentally investigated, based on ASTM D5334-14. The thermal conductivity of granular materials is presented as a function of the porosity and proportion of fine particles. The thermal conductivity tends to be low when the porosity is high and the proportion of fine particles is low (and vice versa). When the fine particles are small enough to fill the pore body of the larger particles, the coordination number increases; thus, the thermal conductivity increases when the proportion of fine particles is high. Therefore, both the porosity and particle size distribution should be carefully considered when the thermal conductivity of mixed silica sand is evaluated.

Keywords: thermal conductivity; silica sand; density; fine content; particle size distribution

1. Introduction

Soils and foundations are modeled as heat sources or sinks in infrastructures, such as geothermal power plants, ground source heat pumps (GSHP), U-shaped borehole heat-exchangers (UBHE), ground heat exchanger piles, and buried pipes for steam or hot water [1–7]. The thermal properties of soil influence the performance of geotechnical structures (such as shallow and deep foundations, pavements, dams, and embankments) against heaving and freezing propagation [8,9]. In addition, the thermal properties of soils have become more important in the design of general infrastructures because of heat-related issues in urban areas (such as heat islands, which are receiving increased attention from the public).

It is well known that the amount of fine particles in granular materials influences engineering properties such as stiffness, strength, and hydraulic conductivity [10,11]. For example, the shear stiffness of granular materials increases with a larger proportion of fine contents at a constant porosity [10]. However, our knowledge on the thermal properties as a function of the proportion of fine particles is limited. In this study, the thermal conductivity (one of the important thermal properties of silica sand) with the varying porosity and proportion of fine particles is experimentally investigated. A transient method (ASTM D5334-14) was used to evaluate the thermal properties of mixed silica sands.

2. Thermal Properties

Thermal properties such as heat capacity, thermal conductivity, thermal expansion, and thermal stress are required to model the heat transfer in soils [12,13]. Heat capacity is the measurable physical energy required to increase the temperature of a material by 1 °C. Thermal conductivity is the ability of a material to conduct heat from high- to low-temperature regions. Thermal expansion is the change in volume of a material in response to a change in temperature. Thermal stress is the change in stress of a material owing to a change in temperature.

Thermal conductivity plays an important role in heat transfer; for example, heat transfers at a low rate in a material with low thermal conductivity. As such, a material with low thermal conductivity can be used for thermal insulation, whereas a material with high thermal conductivity can be used as a heat sink. Thermal conductivity is a property explaining the conduction, convection, and radiation in granular materials [14]. Conduction is affected by the properties of the mineral and the contact area between particles; convection is related to the properties of the fluid filling the sediment pores; and radiation is related to the propagation of heat without any medium [14]. Thus, thermal conductivity depends on the porosity, mineral type, effective stress, saturation, and properties of the pore fluid. For example, thermal conductivity increases with a decrease in porosity, an increase in effective stress, and an increase in degree of water saturation [15–20].

The thermal conductivity of granular materials can be estimated using a steady state or transient method. In the steady state method, the thermal conductivity is evaluated based on Fourier's law for heat conduction, according to Equation (1):

$$\lambda = \frac{Q \cdot L}{A \cdot (T_2 - T_1)} \quad (1)$$

where λ is the thermal conductivity (W/(m·K)), Q is the amount of heat passing through a cross section of the specimen (W), A is the cross-sectional area of the specimen (m²), L is the length of the specimen (m), and T_2 and T_1 are the temperatures at two locations (K).

In the transient method, the thermal conductivity of a material is evaluated based on the change in temperature over time (after heat generation). It normally takes less time to conduct a test using the transient method than to apply the steady state method; therefore, the moisture migration in the material during the test may be minimized [21]. The temperature change ΔT (K) at time t (s), when heating starts at $t = 0$ and stops at $t = t_p$, can be represented through Equations (2) and (3) (ASTM D5334-14):

$$\Delta T = -\frac{Q}{4\pi\lambda} \text{Ei}\left(\frac{-r^2}{4Dt}\right) \quad 0 < t \leq t_p \quad (2)$$

$$\Delta T = -\frac{Q}{4\pi\lambda} \left[-\text{Ei}\left(\frac{-r^2}{4Dt}\right) + \text{Ei}\left(\frac{-r^2}{4D(t-t_p)}\right) \right] \quad t > t_p \quad (3)$$

where, Q is the heat applied per unit length of the heater (W/m), r is the distance from the heat source (m), and D is the thermal diffusivity (m²/s). Equations (2) and (3) can be simplified (using a non-linear least-squares inversion method) into Equations (4) and (5), which are the basis for the evaluation of thermal conductivity using the transient method (ASTM D5334-14):

$$\Delta T = \frac{Q}{4\pi\lambda} \ln(t) \quad 0 < t \leq t_p \quad (4)$$

$$\Delta T = \frac{Q}{4\pi\lambda} \ln\left(\frac{t}{t-t_p}\right) \quad t > t_p \quad (5)$$

Jafari and Jung [22] developed two theoretical models (the parallel and series models) for the thermal conductivity of a soil matrix composed of soil, water, and air. They set the parallel model

as the upper bound of thermal conductivity (Equation (6)) and the series model as the lower bound (Equation (7)):

$$\lambda_{\text{mixture}} = \lambda_{\text{solid}} \cdot (1 - n) + S \cdot \lambda_{\text{water}} \cdot n + (1 - S) \cdot \lambda_{\text{air}} \cdot n \quad (6)$$

$$\lambda_{\text{mixture}} = \frac{1}{\left(\frac{1-n}{\lambda_{\text{solid}}}\right) + \left(\frac{S}{\lambda_{\text{water}}}\right) + \left(\frac{1-S}{\lambda_{\text{air}}}\right)} \quad (7)$$

where, λ_{mixture} , λ_{solid} , λ_{water} , and λ_{air} are the thermal conductivities of the soil matrix (mixture), solid mineral, water, and air, respectively; n is the porosity; and S is the degree of saturation. According to Equations (6) and (7), thermal conductivity is proportional to degree of water saturation, but inversely proportional to porosity. They also considered the Hashin-Shtikman models [22,23] as the upper (Equation (8)) and lower (Equation (9)) bounds of thermal conductivity:

$$\lambda_{\text{mixture}} = \lambda_{\text{solid}} \cdot \left[1 + \frac{3(1-n)(\lambda_{\text{VU}} - \lambda_{\text{solid}})}{3\lambda_{\text{solid}} + n(\lambda_{\text{VU}} - \lambda_{\text{solid}})} \right], \quad (8)$$

where $\lambda_{\text{VU}} = \lambda_{\text{water}} \cdot \left[1 + \frac{3(1-S)(\lambda_{\text{air}} - \lambda_{\text{water}})}{3\lambda_{\text{water}} + S(\lambda_{\text{air}} - \lambda_{\text{water}})} \right]$ and,

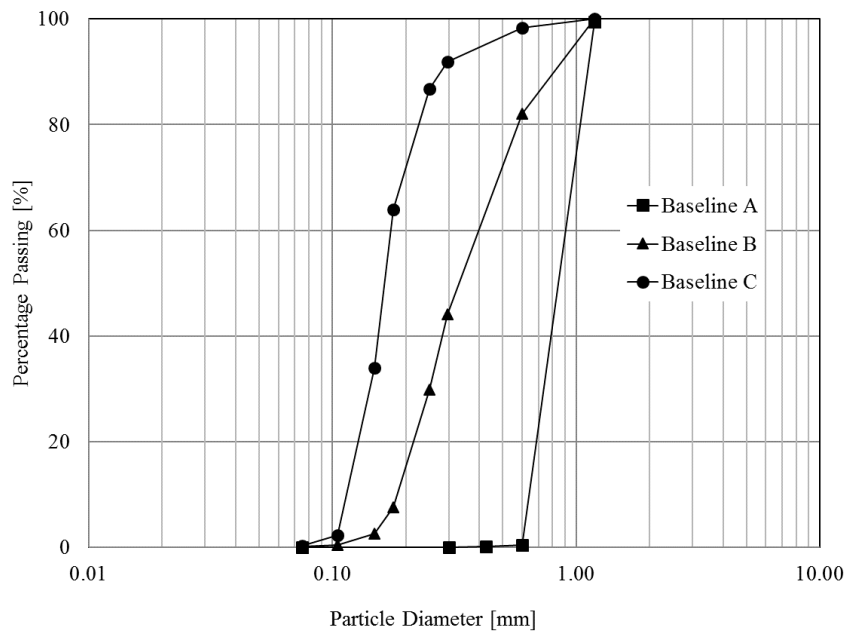
$$\lambda_{\text{mixture}} = \lambda_{\text{VL}} \cdot \left[1 + \frac{3n(\lambda_{\text{solid}} - \lambda_{\text{VL}})}{3\lambda_{\text{VL}} + (1-n)(\lambda_{\text{solid}} - \lambda_{\text{VL}})} \right] \quad (9)$$

where $\lambda_{\text{VL}} = \lambda_{\text{air}} \cdot \left[1 + \frac{3S(\lambda_{\text{water}} - \lambda_{\text{air}})}{3\lambda_{\text{air}} + (1-S)(\lambda_{\text{water}} - \lambda_{\text{air}})} \right]$.

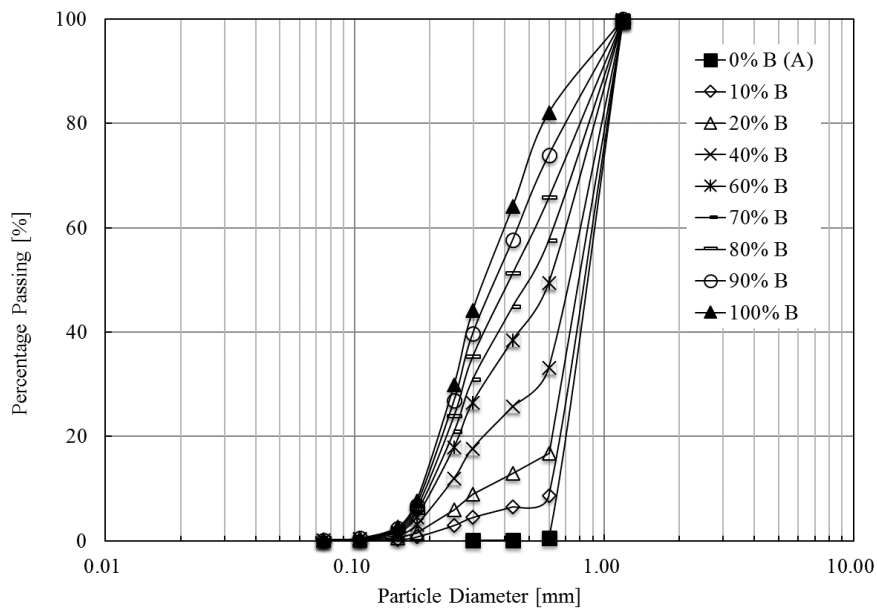
3. Experimental Study

3.1. Materials

Three samples of poorly graded silica sands (samples A, B, and C) were selected as baseline materials for the experiments. The coefficients of curvature (i.e., $C_c = D_{30}^2 / (D_{10} \cdot D_{60})$) of samples A, B, and C were 0.93, 0.86, and 1.03, respectively, and their coefficients of uniformity (i.e., $C_u = D_{60} / D_{10}$) were 1.41, 2.17, and 1.51, respectively. The particle-size distribution curves of the three samples are shown in Figure 1a, and the mean particle sizes (D_{50}) of samples A, B, and C were 0.84, 0.33, and 0.16 mm, respectively. The particle shapes were all bulky and round. Sample A indicates large particles, while samples B and C are designated as fine particles in this article. In an attempt to explore the effect of fine particles on the thermal conductivity of mixed granular materials, two baseline samples (samples A and B, or samples A and C) were mixed with varying proportions of fine particles (B and C), as shown in Figure 1b,c. The labels in Figure 1b,c represent the mixing proportion of the fine particles B and C, respectively. For example, the 80% label in Figure 1b refers to a mixed specimen with 80% of fine particles B and 20% of large particles A in weight, whereas the 0% label indicates a pure sample A without mixing of fine particles B. As shown in the figure, two baselines (100% sample A and 100% sample B) and 12 mixed specimens (A–B and A–C mixed specimens) were considered in this study. The initial void ratio of the 100% sample C was much higher than that of the others, and therefore the thermal conductivity of the 100% sample C was not comparable. Thus, the results of the 100% sample C are not presented in this paper. All tests were conducted using dry specimens, but the effects of water were not within the scope of this study.

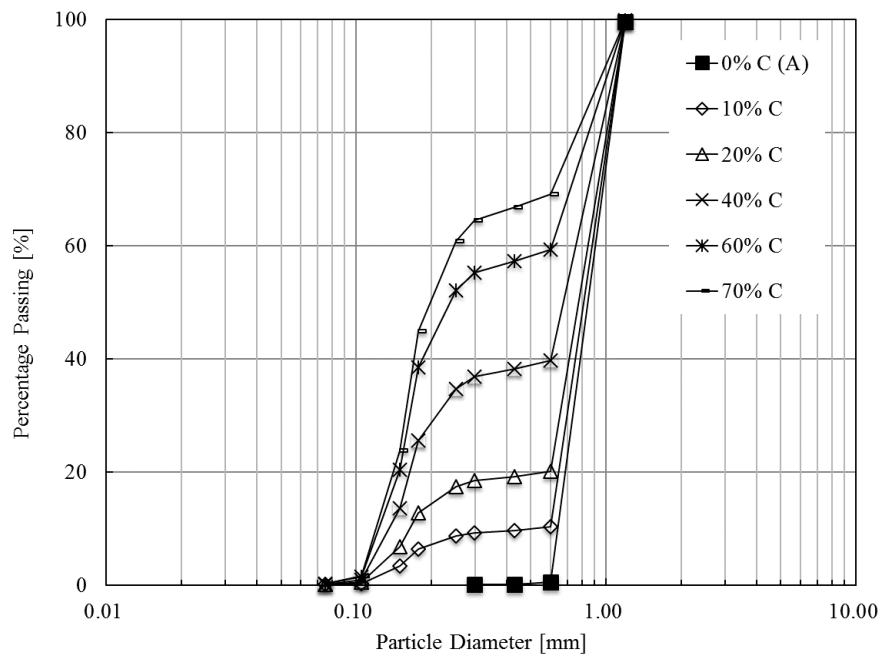


(a) Baseline samples



(b) Mixed specimens of baselines A and B

Figure 1. Cont.



(c) Mixed specimens of baselines A and C

Figure 1. Particle size distributions.

3.2. Experiment Procedure

The tests for thermal conductivity were conducted based on the transient method, ASTM D5334-14, with a needle probe from the East 30 Sensors Company (Pullman, WA, USA). The transient method has the advantage that, owing to its short test duration, the moisture migration in the materials can be minimized compared to that in the steady state method [21]. Figure 2 shows a schematic of the experiment setup [22]. The length of the needle probe was 60 mm and its aspect ratio was larger than 20. The dimensions of the needle probe were sufficient to generate a radial thermal transfer. The needle probe consisted of a heating wire to raise the temperature of the materials and a thermocouple to measure the change in temperature. The heating wire was connected to a DC (direct current) power supply and an amperage meter. The thermocouple was connected to a data logger for recording the temperature at every second during the tests.

The specimens were placed in a transparent polyethylene cylinder with a 10.1 cm inner diameter and 9.3 cm height, and the needle probe was inserted vertically into the materials (Figure 2). They were kept in a room at a constant temperature until the temperature in the specimens became stable ($24 \pm 1 \text{ }^\circ\text{C}$). After setting up the specimens, heat was generated by heating the wire for 1 min. The curve of temperature change versus time at the natural logarithm scale was plotted using the data measured during the heating process. The linear relationship between temperature and time can be used to estimate the thermal conductivity λ of the specimen using Equation (10):

$$\lambda = - \frac{I^2 \times R_m}{4\pi} \times \frac{\ln\left(\frac{t_2}{t_1}\right)}{T_2 - T_1} \times \frac{1}{L} \tag{10}$$

where λ is the thermal conductivity of the specimen (W/mK), I is the electrical current (A), R_m is the electrical resistance of the heated wire (70 Ω in this study), T_1 and T_2 are the temperatures (K) at times t_1 and t_2 , respectively, and L is the length of the needle (m).

Through compaction of the specimens, there was an attempt to achieve a uniform density, and as a result, the initial void ratio of the specimens was between 0.600 and 0.609 for all cases (Figure 3). To change the porosity of the samples, and eventually explore the impact of the porosity and the

proportion of fine particles on the thermal conductivity during the tests, the specimens were loaded one-dimensionally in the cylinder at 12.5 to 1600 kPa with a constant load incremental ratio ($LIR = 1$), using a GeoJac automated loading system (Geotechnical Test Acquisition & Control). The loading interval was 30 min, which was determined through preliminary tests (most of the settlements were completed within 2 to 5 min). At the end of each loading step, the thermal conductivity was measured three times at different specimen locations, and the measurements obtained were very close. This paper presents the average of the three measurements.

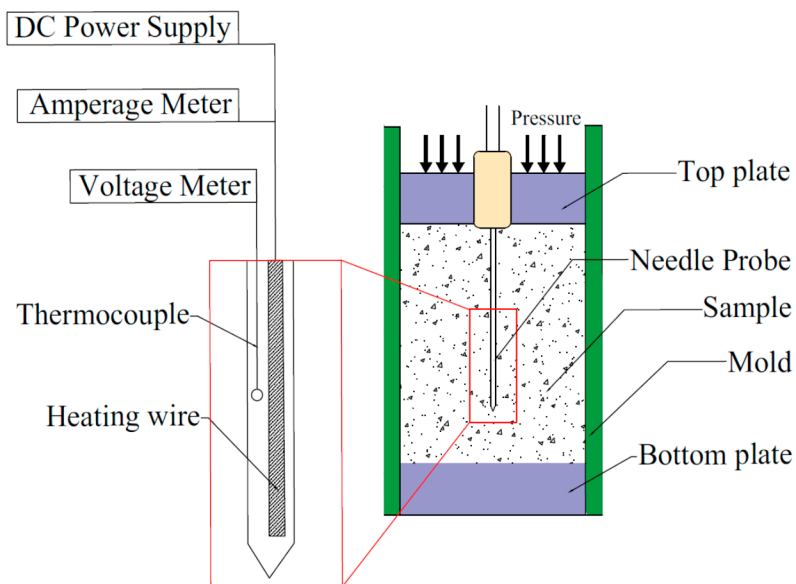
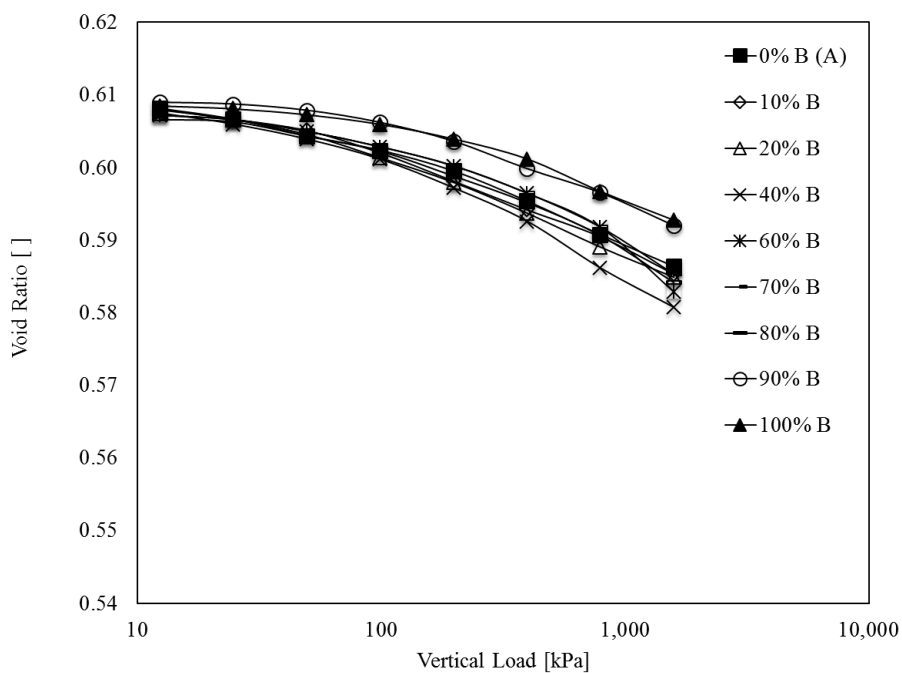
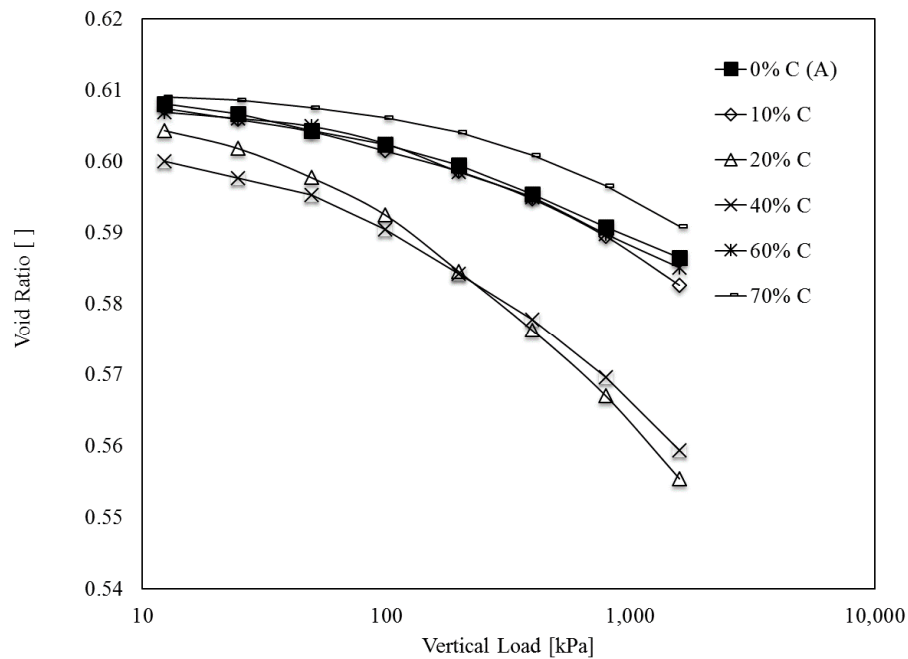


Figure 2. Schematic of experiment setup [22] (copyright, 2015, American Society of Civil Engineers).



(a) Mixed specimens of baselines A and B

Figure 3. Cont.



(b) Mixed specimens of baselines A and C

Figure 3. Void ratio with respect to one-dimensional load.

4. Results and Discussion

4.1. Void Ratio with Change in Vertical Effective Stress

Figure 3 shows the compressional behavior of the specimens under one-dimensional loads. At a vertical effective stress of 12.5 kPa, all the A–B mixed specimens started from a void ratio of approximately 0.608 and presented a similarly decreasing void ratio with increasing load (although the mixed specimens including 90% or 100% of fine particles B were less compressed than the others (Figure 3a)). For A–C mixed specimens, the specimens with 20% and 40% of fine particles C started from a low initial void ratio ($e = 0.600$ – 0.604) and showed significant decreases in the void ratio, whereas the others showed a higher initial void ratio and lower compression (Figure 3b).

The theoretical pore body size of a simple cubic packing of spherical particles equals $0.414D$, which can be considered the loosest packing (Figure 4a). In addition, the pore body size of the cubic tetrahedral packing of spherical particles equals $0.155D$, which can be theoretically considered the densest packing (in Figure 4b, note that D indicates the diameter of the largest particles) [24]. Silica sand, with a void ratio of $e = 0.49$ – 0.79 , has been considered a material with a loose density [25]. Given the initial void ratio and particle size of the baseline specimen A (i.e., 0% B or 0% C), $e = 0.608$, and $D_{50} = 0.84$ mm, respectively, its theoretically expected maximum pore body size is approximately 0.348 mm, which is obtained from $0.414D$. Considering the particle size distribution of fine particles B and C in Figure 1, they have D_{50} values of 0.33 and 0.16 mm, respectively. Fine particles C may easily fill the pore spaces in sample A. As such, the large particles of sample A form the structural skeleton, and the fine particles C in a range of 20% to 40% may be appropriate amount to fill the pore body constructed by sample A and therefore decrease the void ratio of mixed specimens (see Figure 3b). In addition, a change in compressional load increases both the coordination number and the contact area of the particles, thereby decreasing the porosity (or void ratio), which has been consistently reported in the literature [26–28].

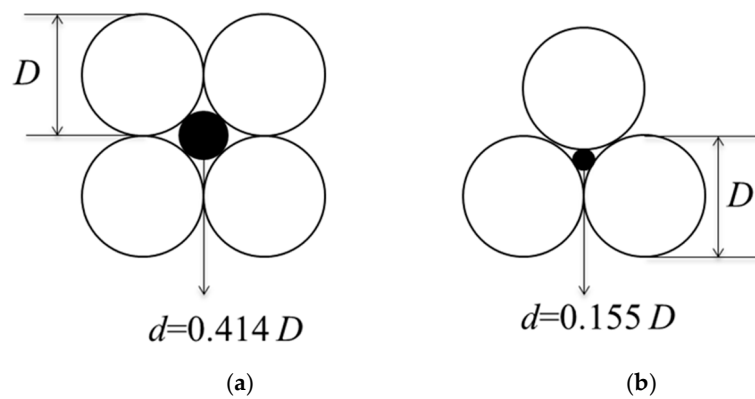


Figure 4. Theoretical pore body sizes of soil packing (D and d are a diameter of the host and fine particles, respectively): (a) the loosest simple cubic packing and (b) the densest tetrahedral packing.

4.2. Thermal Conductivity with Change in Vertical Effective Stress

Figure 5 shows the change in thermal conductivity of the mixed specimens under a one-dimensional compression. It is noted that the thermal conductivity increases with the increase in load. Previous studies have also shown that increased vertical effective stress raises the thermal conduction between particles [26–28]. In Figure 5a, the 0% B specimen (that is, 100% sample A) shows the lowest thermal conductivity along the entire range of loads (because this specimen is the most uniform among all specimens (see Figure 1a) and has the lowest coordination number). The thermal conductivities of the A–B mixed specimens show similar trends and values, except within the range of 0% to 10% of fine particles B. In comparison to the A–B mixed specimens, the smaller size of the fine particles C influence more clearly the thermal conductivity of the A–C mixed specimens up to 40% of fine particles C.

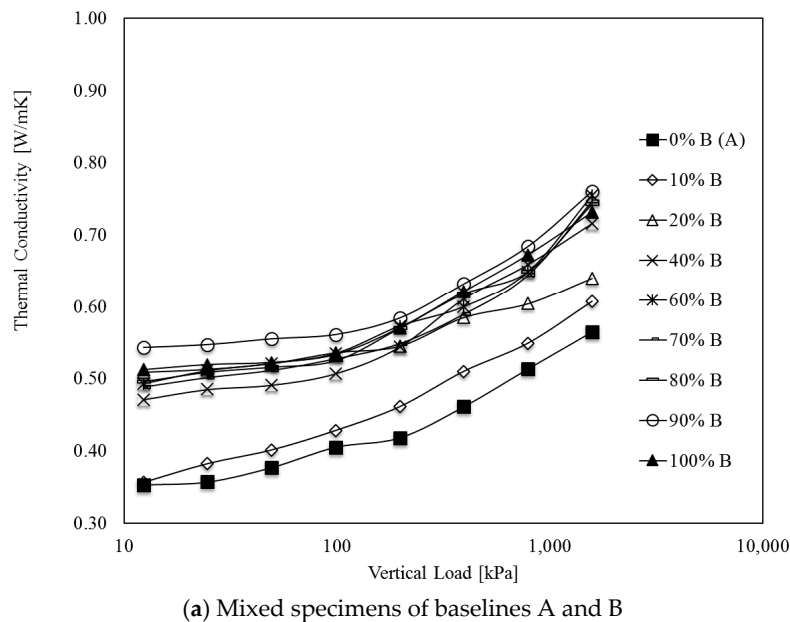
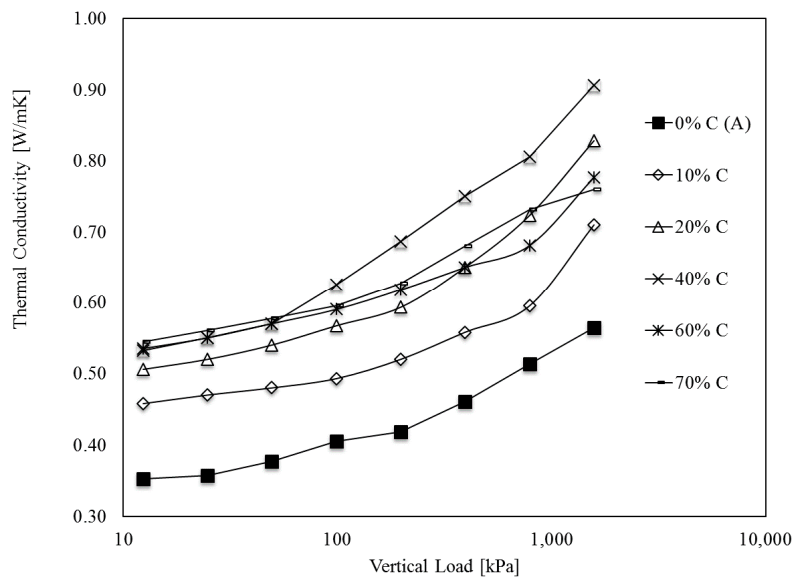


Figure 5. Cont.

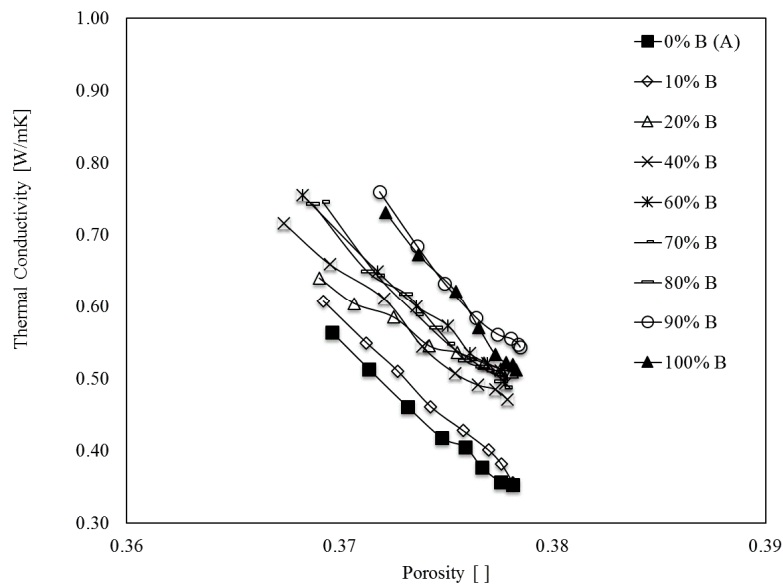


(b) Mixed specimens of baselines A and C

Figure 5. Thermal conductivity with respect to one-dimensional load.

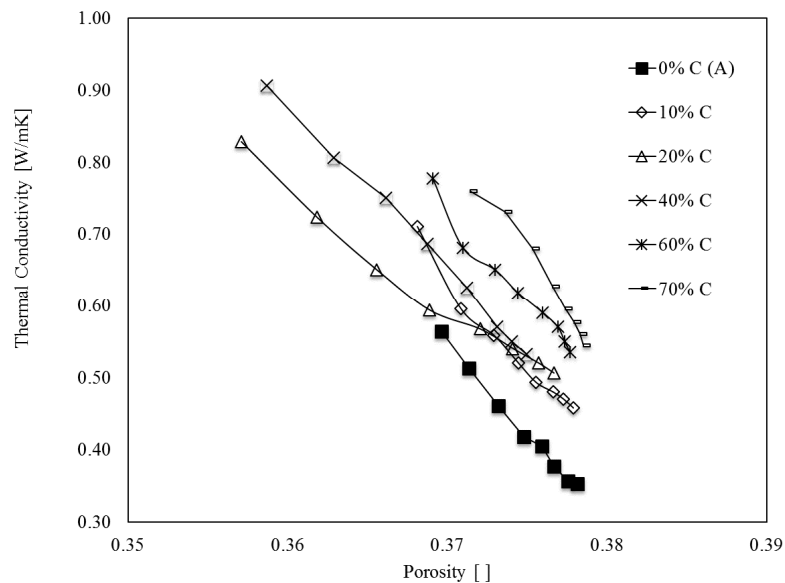
4.3. Thermal Conductivity with Change in Porosity and Fine Particle Contents

Figure 6 shows the variation in thermal conductivity of the baseline and mixed specimens with changes in porosity. The variation in initial porosities results from the particle shape, grain size distribution, and chemical composition of the surfaces, even under the same compaction energy. In general, the thermal conductivity increases with a decrease in porosity for all samples, which is consistent with previously published data [14,16,29]. When the initial porosity is high, the coordination number has a greater influence on the decrease in porosity than the contact area [30]. However, at a low initial porosity, the change in contact area is more significant, affecting the thermal conductivity more [30]. This implies that the increased effective stress results in a larger coordination number and contact area, which causes a decrease in porosity and an increase in thermal conductivity.



(a) Mixed specimens of baselines A and B

Figure 6. Cont.



(b) Mixed specimens of baselines A and C

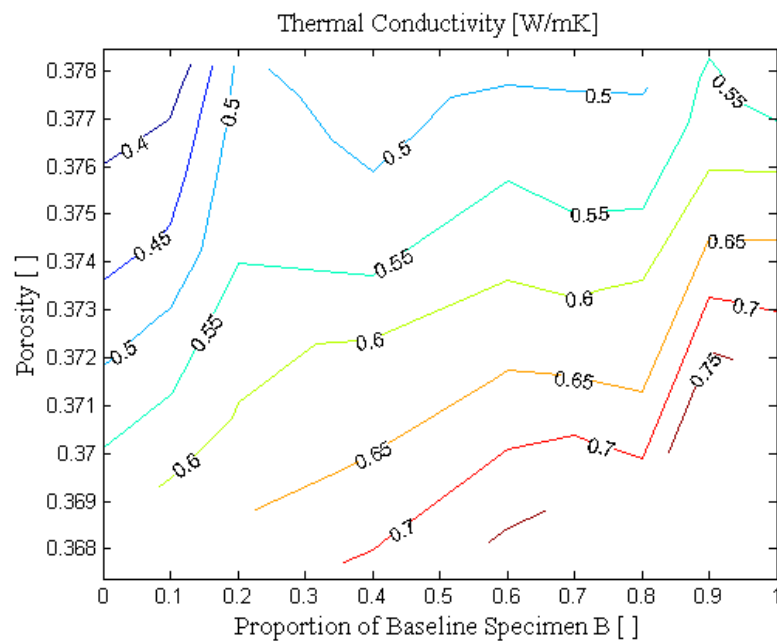
Figure 6. Thermal conductivity with respect to porosity.

For the A–B mixed specimens in Figure 6a, the thermal conductivity of specimens containing 10% to 100% of fine particles B is higher than that of the 100% sample A. However, the effect of the fine particle contents on thermal conductivity of the 20% to 80% B specimens does not seem straightforward. The fine particles B may fill the pore body of the baseline A for fine contents of up to 10%. But for fine contents of 20% or more, the fine particles B may replace particles of the baseline A instead of filling the voids (because the size of fine particles B ($D_{50} = 0.33$ mm) is not much smaller than the size of the pore body of specimen A). Note that the expected pore body size of sample A is 0.348 mm.

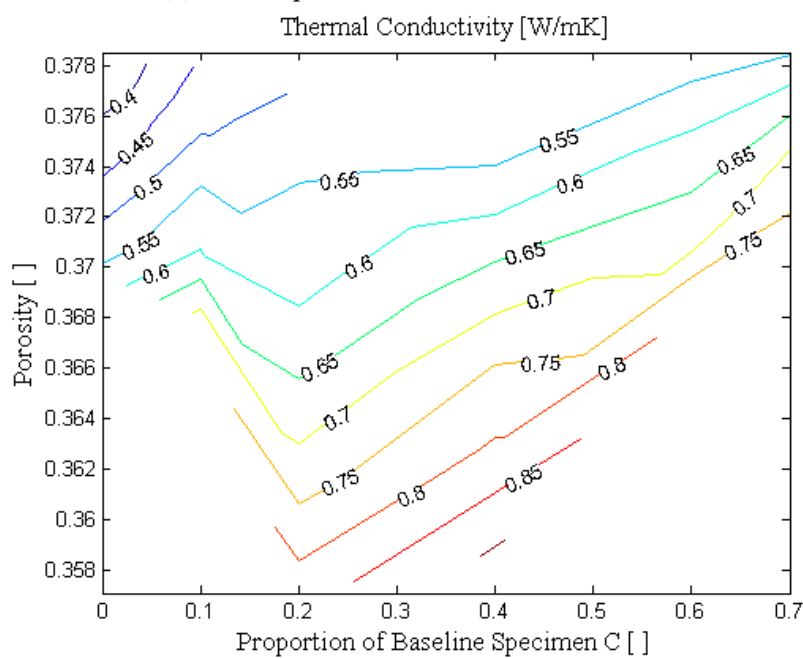
On the other hand, the A–C mixed specimens show a clear trend, and the thermal conductivity of the mixed specimens increases with an increase in fine particles C. The relatively smaller fine particles C ($D_{50} = 0.16$ mm, as shown in Figure 1) seem to fill better the pore body of baseline A. The decrease in pores (by adding fine particles C) causes the thermal conductivity to rise.

An attempt was made to relate the thermal conductivity of a mixed specimen to the properties representing the size and packing of the particles. Various properties such as porosity, coefficient of uniformity, and coefficient of curvature were investigated, but porosity showed better correlation than the other properties. The results of the trials are not presented herein.

Figure 7 shows contours of thermal conductivity as a function of porosity and a proportion of B or C fine particles. The label of the contour indicates the thermal conductivity of the mixed specimens. From the plots, the effects of the porosity and proportion of fine particles can individually be investigated. The results indicate the following. First, the thermal conductivity tends to increase under the lower porosity and higher proportion of fine granular materials (i.e., fine particles B or C), and vice versa. Second, compared to the A–B mixed specimens, the thermal conductivity of the A–C mixed specimens show a clearer trend of increasing thermal conductivity, with increasing proportion of fine particles C (Figure 7b). The sizes of the fine particles C are much smaller than the theoretical pore body size of sample A (D_{50} of sample C is 0.16 mm, and the expected pore body size of sample A is equal to 0.348 mm, based on Figure 4a). The fine particles C (which are smaller than particles B) may effectively fill the pore space in sample A, elevating the coordination. The heating energy can transfer better with the heightened coordination number; the increase in fine particles C results in larger thermal conductivity.



(a) Mixed specimens of baselines A and B



(b) Mixed specimens of baselines A and C

Figure 7. Thermal conductivity as a function of porosity and proportion of fine particles.

However, the size of fine particles B ($D_{50} = 0.33$ mm) is similar to the theoretical estimate of the size of the pore body of sample A. The fine particles B may replace the particles of sample A rather than fill the voids, and therefore the increment in fine particles B does not necessary lead to a raise in thermal conductivity.

5. Conclusions

The thermal conductivity of silica sand, with a varying porosity and proportion of fine particles, was experimentally investigated based on a transient method.

A larger compressional load increases both the coordination number and contact area of the samples and decreases their porosity (or void ratio). Thus, the thermal conductivity also increases with increments in load, which coincides with the results reported in the literature. The most uniformly graded specimen showed the lowest thermal conductivity, which can be explained by the low coordination number of the uniformly packed particles.

This study attempted to relate the thermal conductivity of different samples to the properties representing the size and packing of their particles. The thermal conductivity was presented as a function of porosity and a proportion of fine particles. It was found that the thermal conductivity tends to decrease under a high porosity and a low proportion of fine particles, and vice versa. When the size of the smaller particles is adequate for filling the pore body of the larger particles, the coordination number becomes greater with a larger proportion of fine particles, which causes the thermal conductivity to increase. On the contrary, when the size of the fine particles is not appropriate for filling the pore body of the large particles, the effects of fine contents on thermal conductivity is not straightforward. Thus, both the porosity and particle size distribution should be carefully considered when the thermal conductivity of mixed silica sand is evaluated.

Acknowledgments: This work was supported by a Korean Agency for Infrastructure Technology Advancement (KAIA) grant, funded by the Ministry of Land, Infrastructure, and Transport (Grant 1615007273).

Author Contributions: Jongwon Jung conceived, designed, and conducted the experiments. Jongwon Jung and Jaehun Ahn analyzed the data and wrote the paper. All authors read and approved the final manuscript.

Conflicts of Interest: The authors declare no conflicts of interest.

References

1. Simms, R.B.; Haslam, S.R.; Craig, J.R. Impact of soil heterogeneity on the functioning of horizontal ground heat exchangers. *Geothermics* **2014**, *50*, 35–43. [[CrossRef](#)]
2. Liang, N.-W.; Lai, C.-H.; Hsu, C.-Y.; Chiang, Y.-C.; Chang, C.-C.; Chen, S.-L. A conformal-mapping method for predicting the thermal properties of U-shaped borehole heat-exchangers. *Geothermics* **2014**, *50*, 66–75. [[CrossRef](#)]
3. Yu, K.L.; Singh, R.M.; Bouazza, A.; Bui, H.H. Determining Soil Thermal Conductivity through Numerical Simulation of a Heating Test on a Heat Exchanger Pile. *Geotech. Geol. Eng.* **2015**, *33*, 239–252. [[CrossRef](#)]
4. Kramer, C.; Ghasemi-Fare, O.; Basu, P. Laboratory Thermal Performance Tests on a Model Heat Exchanger Pile in Sand. *Geotech. Geol. Eng.* **2015**, *33*, 253–271. [[CrossRef](#)]
5. Perpar, M.; Rek, Z.; Bajric, S.; Zun, I. Soil thermal conductivity prediction for district heating pre-insulated pipeline in operation. *Energy* **2012**, *44*, 197–210. [[CrossRef](#)]
6. Dalla Rosa, A.; Li, H.; Svendsen, S. Method for optimal design of pipes for low-energy district heating, with focus on heat losses. *Energy* **2011**, *36*, 2407–2418. [[CrossRef](#)]
7. Lee, S.-J.; Kim, K.-Y.; Choi, J.-C.; Kwon, T.-H. Experimental investigation on the variation of thermal conductivity of soils with effective stress, porosity, and water saturation. *Geomech. Eng.* **2016**, *11*, 771–785. [[CrossRef](#)]
8. Pei, W.; Yu, W.; Li, S.; Zhou, J. A new method to model the thermal conductivity of soil–rock media in cold regions: An example from permafrost regions tunnel. *Cold Reg. Sci. Technol.* **2013**, *95*, 11–18. [[CrossRef](#)]
9. Andrianov, I.V.; Starushenko, G.A.; Danishevskii, V.V. Asymptotic determination of the effective thermal conductivity of a pile field. *Soil Mech. Found. Eng.* **1999**, *36*, 31–36. [[CrossRef](#)]
10. Choo, H.; Lee, W.; Lee, C. Compressibility and small strain stiffness of kaolin clay mixed with varying amounts of sand. *KSCE J. Civ. Eng.* **2016**. [[CrossRef](#)]
11. Choo, H.; Kim, J.; Lee, W.; Lee, C. Relationship between hydraulic conductivity and formation factor of coarse-grained soils as a function of particle size. *J. Appl. Geophys.* **2016**, *127*, 91–101. [[CrossRef](#)]
12. Skinner, B.J. Thermal expansion. *Mem.—Geol. Soc. Am.* **1966**, *97*, 75–96.
13. Eppelbaum, L.; Kutasov, I.; Pilchin, A. Thermal Properties of Rocks and Density of Fluids. *Appl. Geotherm.* **2014**, 99–149. [[CrossRef](#)]
14. Yun, T.S.; Santamarina, J.C. Fundamental study of thermal conduction in dry soils. *Granul. Matter* **2008**, *10*, 197–207. [[CrossRef](#)]

15. Barry-Macaulay, D.; Bouazza, A.; Singh, R.M.; Wang, B.; Ranjith, P.G. Thermal conductivity of soils and rocks from the Melbourne (Australia) region. *Eng. Geol.* **2013**, *164*, 131–138. [[CrossRef](#)]
16. Côté, J.; Konrad, J.-M. Thermal conductivity of base-course materials. *Can. Geotech. J.* **2005**, *42*, 61–78. [[CrossRef](#)]
17. Lu, Y.; Lu, S.; Horton, R.; Ren, T. An Empirical Model for Estimating Soil Thermal Conductivity from Texture, Water Content, and Bulk Density. *Soil Sci. Soc. Am. J.* **2014**, *78*, 1859–1868. [[CrossRef](#)]
18. Kömle, N.; Hütter, E.; Feng, W. Thermal conductivity measurements of coarse-grained gravel materials using a hollow cylindrical sensor. *Acta Geotech.* **2010**, *5*, 211–223. [[CrossRef](#)]
19. Abuel-Naga, H.M.; Bergado, D.T.; Bouazza, A.; Pender, M.J. Thermal conductivity of soft Bangkok clay from laboratory and field measurements. *Eng. Geol.* **2009**, *105*, 211–219. [[CrossRef](#)]
20. Ochsner, T.E.; Horton, R.; Ren, T. A New Perspective on Soil Thermal Properties. *Soil Sci. Soc. Am. J.* **2001**, *65*, 1641–1647. [[CrossRef](#)]
21. Abdel-Wahed, R.M.; Pfender, E.; Eckert, E.R.G. A Transient Method for Measuring Thermal Properties of Soils. *Wärme Stoffübertrag* **1987**, *11*, 1–8. [[CrossRef](#)]
22. Jafari, M.; Jung, J. Thermal properties of fly ashes and biomass ashes including wood- and sugarcane ashes. *J. Mater. Civ. Eng. (ASCE)* **2017**, *29*. [[CrossRef](#)]
23. Hashin, Z.; Shtrikman, S. A variational approach to the theory of the effective magnetic permeability of multiphase materials. *J. Appl. Phys.* **1962**, *33*, 3125–3131. [[CrossRef](#)]
24. Grau, F.; Choo, H.; Hu, J.W.; Jung, J. Engineering behavior and characteristics of wood ash and sugarcane bagasse ash. *Materials* **2015**, *8*, 6962–6977. [[CrossRef](#)]
25. Hough, B.K. *Basic Soils Engineering*; The Ronald Press Company: New York, NY, USA, 1957; p. 513.
26. Cortes, D.D.; Martin, A.I.; Yun, T.S.; Francisca, F.M.; Santamarina, J.C.; Ruppel, C. Thermal conductivity of hydrate-bearing sediments. *J. Geophys. Res. Solid Earth* **2009**, *114*. [[CrossRef](#)]
27. Narsilio, G.A.; Yun, T.S.; Kress, J.; Evans, T.M. Hydraulic and thermal conduction phenomena in soils at the particle-scale: Towards realistic FEM simulations. *IOP Conf. Ser. Mater. Sci. Eng.* **2010**, *10*, 012086. [[CrossRef](#)]
28. Lee, J.; Yun, T.; Choi, S.-U. The Effect of Particle Size on Thermal Conduction in Granular Mixtures. *Materials* **2015**, *8*, 3975–3991. [[CrossRef](#)]
29. Abu-Hamdeh, N.H. Thermal Properties of Soils as affected by Density and Water Content. *Biosyst. Eng.* **2003**, *86*, 97–102. [[CrossRef](#)]
30. Yun, T.S.; Evans, T.M. Three-dimensional random network model for thermal conductivity in particulate materials. *Comput. Geotech.* **2010**, *37*, 991–998. [[CrossRef](#)]



© 2017 by the authors. Licensee MDPI, Basel, Switzerland. This article is an open access article distributed under the terms and conditions of the Creative Commons Attribution (CC BY) license (<http://creativecommons.org/licenses/by/4.0/>).